PCCP

Accepted Manuscript

ROYAL SOCIETY OF CHEMISTRY

www.rsc.org/pccp

Journal Name

ARTICLE

Improved conductivity of $NdFeO_3$ through partial substitution of Nd by Ca: a theoretical study

Received 00th January 20xx,
Accepted 00th January 20xx

DOI: 10.1039/x0xx00000x

www.rsc.org/

You Wang,[a] Yun Wang,[b] Wei Ren,[c] Porun Liu,[b] Huijun Zhao,*[b] Jun Chen,[a] Jinxia Deng,[d] and Xianran Xing*[a]

$NdFeO_3$ is an important candidate materials for gas sensors and intermediate-temperature solid oxide fuel cells (IT-SOFC). However, its low conductivity prohibits its applications. In this study, we report that the doping of Ca by replacing partial Nd can effectively increase its conductivity. Through the electronic structure analysis of $Nd_{1-x}Ca_xFeO_3$ (x=0.00, 0.25, 0.50, 0.75 or 1.00) based on the first-principles density functional theory calculations, it is found the hole states introduced by Ca substitution appear just above the Fermi level, which implies a high mobility of electrons/holes along the Fe-O-Fe bonding network. Specifically, it becomes easier to form O vacancies after Ca doping. Since the diffusion of O anions occurs through a vacancy hopping mechanism, the ion conductivity is also improved. These findings help us to gain an in-depth understanding of the colossal increased conductivity of Ca doped $NdFeO_3$ and turn the electronic conduction for their practical application as gas sensor and IT-SOFC.

Introduction

The perovskite type oxides with the chemical formula ABO_3 (where A is an alkaline-earth or a rare-earth metal and B is a transition metal) represent a particularly interesting class of materials due to their dielectric,[1, 2] magnetic,[3] magneto-optical,[4, 5] multiferric,[6-8] catalytic,[9-11] and gas-sensitive properties.[12, 13] The large variety of properties displayed by ABO_3 is due to the ability of the exceptional tolerance of their framework to accommodate different cations and defects.[14] In the regular perovskite lattice, the smaller B ions are placed in the center of BO_6 octahedra, which are corner-connected to form a three-dimensional (3-D) B-O framework. Each A cation is located in the center of a distorted cubooctahedral pocket with twelve O anions at the vertices, which is enclosed by eight [BO_6] octahedral.[15]

As one of rare earth orthoferrites, $NdFeO_3$ and its derivates have attracted great attentions because they are important candidates as gas sensors and cathode materials for intermediate-temperature solid oxide fuel cells (IT-SOFCs) due to their good chemical, thermal and mechanical stability.[16, 17] As gas sensors, their electrical properties change in response to the introduction of sensor into some gas phase. For example, as a p-type semiconductor, their resistance increases when they are exposed to the surrounding gas like ethanol, acetone, carbon monoxide or hydrocarbon. The sensitivity of gas sensors is the most important parameter to represent their performance, which is defined as the ratio of the electrical resistance in sample gases (R_g) to that in air (R_a). Therefore, the high resistance of $NdFeO_3$ is a serious drawback, because it can reduce the sensitivity and consume high power. On the other hand, when $NdFeO_3$ acts as a cathode material of IT-SOFC, the high mixed ionic and electronic conductivity is also needed. Therefore, the improvement of conductivity of $NdFeO_3$ is highly desired for their practical applications.

Previously, the doping strategy has been successfully adopted to modulate the conductivity of perovskite. Colossal resistance switching and band gap modulation in a perovskite $SmNiO_3$ have been reported by doping with donor elements such as Li and Mg.[18] A reversible resistivity modulation greater than eight orders of magnitude was demonstrated at room temperature. Alkaline-earth doped $LaCoO_3$ has been found to be promising as conductive oxide alternative of standard metals for electrodes. A maximum electrical conductivity, σ = 4.4×10^3 S cm^{-1}, was achieved in $La_{0.6}Sr_{0.4}CoO_3$.[19] For $Nd_xCa_{1-x}FeO_{3-\sigma}$ (x=0.00, 0.25, 0.50, 0.75 or 1.00) system, a resistivity modulation greater than four orders of magnitude was demonstrate at room temperature by Ca doping strategy.[20] $Nd_{0.6}Ca_{0.4}FeO_{3-\sigma}$ has been reported to exhibit fairly high electrical conductivity, over 100 S cm^{-1} at T > 650 ℃.[21] Thus, by a careful doping of lower-valence cations in the A site, the

[a] Department of Physical Chemistry, University of Science and Technology Beijing, Beijing 100083, China, E-mail: xing@ustb.edu.cn, Fax: +86 1062332525, Tel: +86 10 62332525
[b] Centre for clean Environment and Energy and Griffith School of Environment, Griffith University, Gold Coast Campus, QLD 4222, Australian, E-mail: h.zhao@griffith.edu.au, Fax: +61 7 55528067, Tel: +61 7 55528261
[c] Department of Physics, International Center of Quantum and Molecular Structures, and Materials Genome Institute, Shanghai University, Shanghai 200444, China
[d] Department of Chemistry, University of Science and technology Beijing, Beijing 100083, China

manipulation of electronic properties of rare earth transition metal oxides materials is in principle possible for their specific applications. However, the roles of lower-valence cations at the A site and O vacancies in the modulation of conductivities are still unclear. In order to understand the colossally increased conductivity of Ca doped $NdFeO_3$, fundamental insight into the electronic structure and defect chemistry is needed. While magnetic properties and electronic structures of $NdFeO_3$ have been analysed through accurate first principles calculations based on density functional theory,[22, 23] there is no theoretical study focusing on the properties of doped $NdFeO_3$ without or with O vacancies. Herein, the structural and electronic properties of $Nd_{1-x}Ca_xFeO_{3-\delta}$ (x=0.00, 0.25, 0.50, 0.75 or 1.00, δ=0.00 or 0.25) have been investigated using the first principles method. Our results demonstrate that both electron-deficient A-site dopants and O vacancies can improve their conductivity. The comparative data suggest that the influence of O vacancies is stronger. Furthermore, the substitution of Nd by Ca can also benefit the improvement of ionic conductivity through the formation of O vacancies.

Methods and computational details

All density functional theory (DFT) computations were performed using the Vienna ab initio simulation package (VASP) based on the projector augmented wave (PAW) method.[24] Here, the 4f electrons of Nd atoms were kept frozen as core electrons with 11 valence electrons ($5s^25p^65d^16s^2$), and the valence configurations are $3s^23p^64s^2$, $3d^74s^1$ and $2s^22p^4$ for Ca, Fe and O, respectively. A plane-wave basis set was employed to expand the smooth part of wave functions with a kinetic energy cut-off of 520 eV. For the electron-electron exchange and correlation interactions, the Perdew- Burke-Ernzerhof type functional (PBE),[25] a form of the general gradient approximation (GGA), was used throughout the calculations with the consideration of spin-polarization. Due to insufficient consideration of the on-site Columbic repulsion between the Fe d electrons, GGA-DFT may fail to describe the electronic structure of the $NdFeO_3$. To overcome this shortcoming, the GGA+U approach was used.[26] Following previous studies, we chose U-J = 5.0 eV for the Fe atom.[22]

We performed Brillouin-zone integrations using a (6 × 6 × 4) Monkhorst-Pack k-point grid for the supercell of orthorhombic $Nd_xCa_{1-x}FeO_{3-\delta}$ (x=0.00, 0.25, 0.50, 0.75 or 1.00; δ=0.00, 0.25). As shown in Fig. 1, the Nd (or Ca) cation is surrounded by 12 O ions, whereas the Fe cation is embedded in an O octahedron.[28] Two adjacent octahedra are connected by one O ion, which provides the superexchange bond between the two Fe ions.[29] Herein, a G-type antiferromagnetic state was assumed, in which each Fe ion has six nearest neighbour Fe ions with the antiparallel magnetic moments (see Fig. S1).[23] In the geometry optimization, all atoms were allowed to relax. All residual forces were smaller than 0.005 eV/Å after the geometries

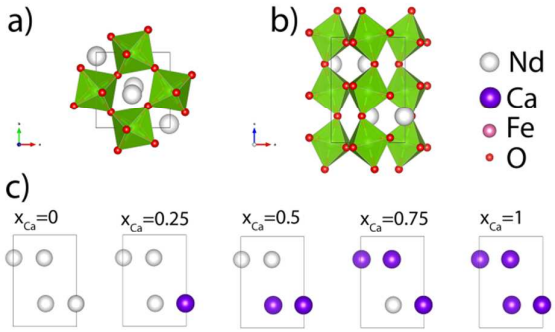

Fig. 1 a) Top view and b) side view of $NdFeO_3$ orthorhombic unit cell. c) Nd/Ca arrangements for x=0.00, 0.25, 0.50, 0.75, 1.00 of $Nd_{1-x}Ca_xFeO_3$ in our DFT calculation. Structures are visualized with VESTA.[27]

were fully optimized, and the computed total energy was converged within 10^{-5}eV.

To understand the doping effect on the formation of a high concentration of charge-compensating O vacancies,[30] the O vacancy formation energy (ΔE_{Vo}) was calculated as:

$$\Delta E_{Vo} = E_{defective} - E_{perfect} + 1/2\ Eo_2 \quad (1)$$

The $E_{defective}$ and $E_{perfect}$ are the energies of the systems with (one neutral O atom removed) and without (perfect) the O vacancies, respectively. The Eo_2 is referenced to the ground state of an optimized O_2 molecule calculated at the same level of theory. We neglected the contributions from the finite temperature entropies including the vibrations of crystalline lattice and O_2 (and the rotations and translations of O_2) as well as configurational entropy for simplicity. As the temperature rises, it is expected to lower the free energy of formation of vacancies.[31]

Results and discussion

Previous experiments have demonstrated that the doping of Ca^{2+} cations can significantly reduce the resistance of $NdFeO_3$.[20] To understand the origin of this colossal reduction of resistance, first-principles theoretical analysis of the electronic structure of the $Nd_xCa_{1-x}FeO_3$ (x=0.00, 0.25, 0.50, 0.75 or 1.00) was conducted. First, we have validated the computational parameters by comparing their magnetic properties of antiferromagnetic $NdFeO_3$ with GGA and GGA+U methods. It is found that the magnetic moment of Fe is 0.05±0.03 μ_B based on the GGA results, in contrast to the experimental data (3.845 μ_B).[32] Using GGA+U method, the local magnetic moments on Fe are 4.087 μ_B in the high spin state, which agrees well with the experimental data. Thus, U-J = 5.0 eV for Fe atoms has been used in the subsequent calculations to analyse their structural and electronic properties.

The substitutions of Nd^{3+} cations by low-valence Ca^{2+} cations with different mole fraction of Ca^{2+} are illustrated in Fig. 1c. For x=0.5, we have considered three types of Ca substitution in

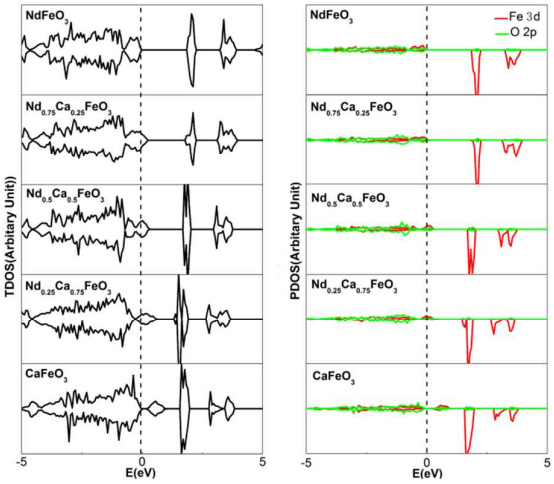

Fig. 2 Total density of states (TDOS) and partial density of states (PDOS) of $Nd_{1-x}Ca_xFeO_3$ (x=0.00, 0.25, 0.50, 0.75, 1.00). The vertical dashed lines represent the position of the Fermi level.

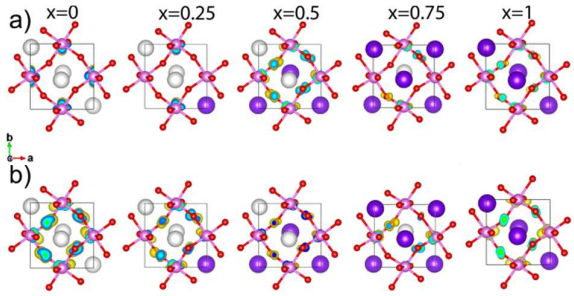

Fig. 3 Charge densities of a) the valence band maximum and b) the conduction band minimum of $Nd_{1-x}Ca_xFeO_3$ (x=0.00, 0.25, 0.50, 0.75, 1.00).

the theoretical study. Their Nd/Ca arrangement and total density of states were calculated (See Fig. S2). While their TDOS were similar, their total energy is -142.19eV, -142.47eV and -142.51eV for model a), b) and c), respectively. So We present the model which has the lowest total energy. For clarity, we only show the arrangements of Nd and Ca from the supercell structures. After the doping of Ca^{2+} cations, the axial Fe-O bond lengths are slightly affected with a maximum deviation of about 0.07 Å (see Fig. S3). The effect of doping on the equatorial Fe-O bond length is much stronger with the maximum deviation as 0.35 Å (see Fig. S4). At the same time, the doping of Ca^{2+} changes the axial O-Fe-O bond angles (see Fig. S5), and the equatorial O-Fe-O bond angles substantially (see Fig. S6). These structural modifications indicate that the doping of Ca^{2+} has greater impacts on the atoms along the equatorial directions.

Since the electronic conductivity of semiconductors is strongly dependent on the band gap,[33] the total density of states (TDOS) and partial density of states (PDOS) of $Nd_{1-x}Ca_xFeO_3$ (x=0.00, 0.25, 0.50, 0.75 or 1.00) were calculated based on the optimized structures (See Fig. 2, S7). The highest occupied state is defined as the Fermi energy, which is set to zero. As shown in Fig. 2, the band gap energy of orthorhombic $NdFeO_3$ is 1.87eV. The PDOS images of Fe 3d and O 2p states are also shown in Fig. 2, because they can provide more details about the contribution of composition to band structures. Since the 3d orbitals of Fe^{3+} ions are half-filled ($t_{2g}^3 \uparrow e_g^2 \uparrow$), the spin-up bands are located below the Fermi energy level and the spin-down states are above the Fermi energy level. Their valance band edge is a complex of O 2p and Fe 3d state, which weakens the localized nature of Fe 3d electrons, whereas the conduction band edge is dominated by the Fe 3d state. Such analysis can also be supported from the charge densities of the valence band maximum and the conduction band minimum of $NdFeO_3$. From Fig. 3, the charge densities of the valence band maximum are around Fe and O atoms. On the other hand, the charge densities of the conduction band minimum are just around Fe atoms in $NdFeO_3$. The ligand-metal charge transfer can take place from the hybridization orbital of Fe 3d and O 2p to the unoccupied Fe 3d orbital by visible light or heat. Our calculation results agree with O K-edge X-ray absorption spectroscopy, which estimates hybridization of transition metal and oxygen state.[34] For x=0.25, 0.50, 0.75, the holes introduced by Ca substitution appear just above the Fermi level. It can be also seen that their charge densities of the conduction band minimum are around Fe and O atoms, which is different from $NdFeO_3$. With more Ca doping, the band gap energies become smaller (See Table 1). Thus, the GGA+U method correctly predicts P-type semi-conductivity for these Ca doped $NdFeO_3$. The octahedral surroundings of the Fe ions can cause their 3d levels to split into t_{2g} and e_g sublevels while O 2p orbitals split $2p_\pi$ and $2p_\delta$ orbitals. The δ-bonds (e_g-p_δ-e_g bonds) resulting from the 3d e_g orbitals of Fe cations and the $2p_\delta$ orbitals of O^{2-} and the π-bonds (t_{2g}-p_π-t_{2g} bonds) are formed with the 3d t_{2g} orbitals of Fe ions and the $2p_\pi$ of O ions.[35] The PDOS images of O 2p, Fe t_{2g} and Fe e_g are shown in Fig. S8. The bands, which are not fully populated and have empty states just above the Fermi level, imply a high mobility of electrons/holes along the Fe-O-Fe bonding network. Therefore, the excess electron density can easily occupy these empty states across the Fermi level, which will lead to charge delocalization.[31] These features are consistent with the high electronic conductivity reported in $La_{1-x}Sr_xFeO_3$.[36] For x=1, a narrow band gap of 0.2 eV is observed. Furthermore, the charge delocalization can be seen from the Bader charge of $Nd_{1-x}Ca_xFeO_3$ (x=0.00, 0.25, 0.50, 0.75 or 1.00). With the increase of the Ca mole fraction, the hole densities arise. However, the Bader charges of Fe and Nd remain essentially unchanged and the Bader charge on O becomes less negative by only 0.04 electrons per O atom (see Table 2). The small difference indicates holes are delocalized on the entire oxygen

Table 1. Energy gap (E_g) of $Nd_{1-x}Ca_xFeO_3$ (x=0.00, 0.25, 0.50, 0.75, 1.00)

x	0.00	0.25	0.50	0.75	1.00
E_g(eV)	1.87	1.53	0.73	0.67	0.20

Table 2. Magnetic moments μ (μ_B) and Bader charges q (e) for $Nd_{1-x}Ca_xFeO_3$ (x=0.00, 0.25, 0.50, 0.75, 1.00) without (M) and with (M*) oxygen vacancy

	X=0.00		X=0.25		X=0.50		X=0.75		X=1.0	
	M	M*	M	M*	M	M*	M	M*	M	M*
μ_{Fe}	4.09	4.06±0.01	3.97±0.09	4.06±0.01	3.84±0.06	4.07	3.51±0.15	4.07±0.01	3.51	3.86±0.22
$\mu_{Fe'}$		3.64±0.06		3.82±0.25		3.99±0.01		3.64±0.31		3.62±0.29
q_{Fe}	1.75	1.73	1.75±0.01	1.73±0.01	1.75	1.73	1.76±0.01	1.72±0.01	1.77	1.74±0.03
$q_{Fe'}$		1.28±0.01		1.45±0.17		1.65±0.01		1.68±0.03		1.69±0.04
q_{Nd}	2.15	2.13±0.02	2.15±0.01	2.11±0.03	2.15	2.13±0.01	2.16	2.12		
q_{Ca}			1.58	1.56	1.58	1.56	1.59	1.57±0.01	1.59	1.58±0.01
q_O	-1.29	-1.31±0.02	-1.25±0.01	-1.29±0.02	-1.2±0.02	-1.28±0.04	-1.16±0.04	-1.21±0.1	-1.12	-1.19±0.07

Table 3. Calculated (DFT+U) formation energies of an oxygen vacancy from $Nd_{1-x}Ca_xFeO_3$(x=0.00, 0.25, 0.50, 0.75, 1.00)

x	0.00	0.25	0.50	0.75	1.00
ΔE_{Vo} (eV)	4.49	2.67	1.07	0.37	0.07

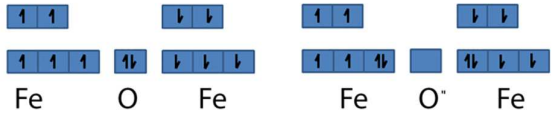

Fig. 4 Schematic of the d orbital occupations with and without an O vacancy in $NdFeO_3$.

sublattice. The introduction of Ca into $NdFeO_3$, therefore, can enhance the electronic conductivity of $NdFeO_3$.

Since acceptor doping of oxides generally results in the formation of charge-compensating O vacancies, we also investigated the structural and electronic properties of $Nd_{1-x}Ca_xFeO_{2.75}$ (x=0.00, 0.25, 0.50, 0.75 or 1.00), by removing one neutral O atom. For $NdFeO_3$, we considered the two unique O vacancies that can be formed: those along axial and equatorial Fe-O-Fe bonds (see Fig. S9). The ΔE_{Vo} (axial) is 4.54eV and the ΔE_{Vo} (equatorial) is 4.48eV, calculated through Eq. 1. The main reason of favourable Fe-*Vo*-Fe equatorial configurations is due to their much weaker Fe-O bond. This is supported by the calculated Fe-O distances, 2.03 Å for the equatorial one and 2.05 Å for the axial one. The larger distance indicates the weaker Fe-O bonds. To this end, only ΔE_{Vo} (equatorial) was considered for the consequent investigation.

From Table 3, the ΔE_{Vo} decreases with the increase of the mole fraction of Ca^{2+}. It suggests that more O vacancies can form with the increase of the mole fraction of Ca^{2+}. By the analysis of the magnetic moment and Bader charges of $Nd_{1-x}Ca_xFeO_{2.75}$ (x=0.00, 0.25, 0.50, 0.75 or 1.00), the decrease of ΔE_{Vo} after the doping of Ca can be understood. After the removal of a neutral O atom, two electrons are left behind. The most significant changes involve the Fe ions adjacent to the O vacancy, where a reduction of charge on these ions is predicted (see Table 2).[37] Fig. 4 shows the electronic states of Fe ions before and after O removal. The anti-ferromagnetically

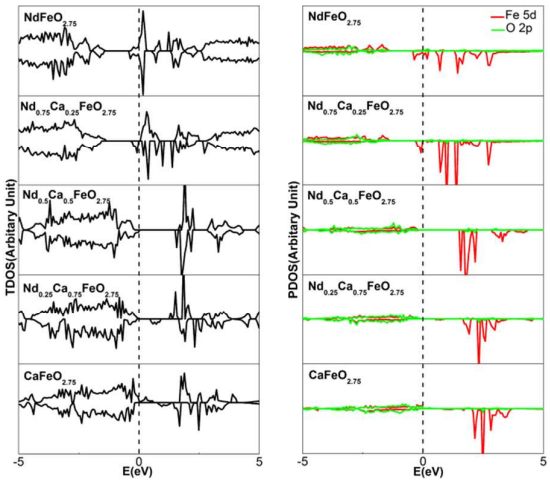

Fig. 5 Total density of states and partial density of states of $Nd_{1-x}Ca_xFeO_{2.75}$(x=0.00, 0.25, 0.50, 0.75, 1.00). The vertical dashed lines represent the position of the Fermi level.

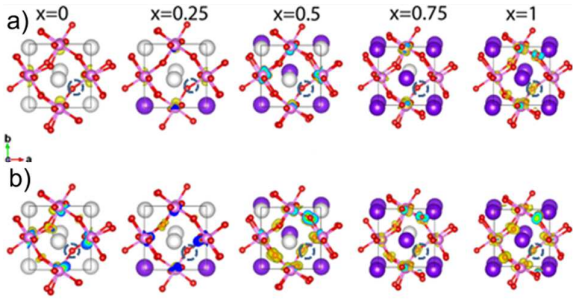

Fig. 6 Charge densities of a) the valence band maximum and b) the conduction band minimum of $Nd_{1-x}Ca_xFeO_{2.75}$ (x=0.00, 0.25, 0.50, 0.75, 1.00).

coupled Fe ions are in the high spin state. Upon the removal of a neutral O atom, the excess electrons in $Nd_{1-x}Ca_xFeO_{2.75}$ (x=0.00, 0.25, 0.50, 0.75 or 1.00) can only occupy antiparallel spin states, producing a decrease in the magnetic moment of Fe ions next to the vacancy (which is defined as Fe' in Table 2). The additional electron-electron repulsion of doubly occupying a d-orbital will give rise to the high ΔE_{Vo}. After the doping of Ca^{2+}, the electron density around the Fe cations adjacent to

the O vacancy is reduced. Additionally, the charges on the other O anions become more negative, which indicates the charge densities created by O vacancies are delocalized. The dispersed electrons compensate the holes arising from Ca^{2+} doping. Therefore, the Fe cation remains in the +3 state with no additional electron-electron repulsion, which leads to a lower ΔE_{Vo}.

Comparing with Fe-O distances after the doping of Ca^{2+} with and without O vacancies, we find that the formation of O vacancies causes larger changes of Fe-O distances than those only with the doping of Ca (see Fig. S3, 4). The same trend is found in Fe-O-Fe angles (see Fig. S5, 6). The TDOS and PDOS of $Nd_{1-x}Ca_xFeO_{2.75}$ (x=0.00, 0.25, 0.50, 0.75 or 1.00) were also investigated (see Fig. 5, S7). For $Nd_{1-x}Ca_xFeO_{2.75}$ (x=0.00, 0.25), the formation of charge-compensating O vacancies make the Fermi level moves towards to conduction band. The DOS of $NdFeO_{2.75}$, $Nd_{0.75}Ca_{0.25}FeO_{2.75}$ and $CaFeO_{2.75}$ show a metallic behavior. As shown in Fig. 5, new states/bands appear around the Fermi level, which are mainly contributed by Fe 3d orbitals hybridized with O 2p orbitals. Their valance band edge is a complex of O 2p and Fe 3d state, whereas the conduction band edge is dominated by the Fe 3d state. It can be also seen from their charge densities of the valence band maximum and the conduction band minimum (see Fig. 6). For x=0.75, a small band gap of 0.47eV is observed. However, we predict $Nd_{0.5}Ca_{0.5}FeO_{2.75}$ has a large resistance with band gap of 1.47eV for balanced charge, since the O vacancies act as electron donors and the doped Ca act as electron acceptors. The trend of conductivity of $Nd_{1-x}Ca_xFeO_{2.75}$ (x=0.00, 0.25, 0.50, 0.75 or 1.00) is in qualitatively agreement with the experiments results of Yo et al., which found their conductivity first increased with Ca substitution then decreased.[20]

It has been reported $Nd_{1-x}Ca_xFeO_{3-\sigma}$ compounds exhibit the characteristic of a mixed ion-electron conductivity.[21] The diffusion of O anions occurs through a vacancy hopping mechanism in perovskite-type transition metal oxides, so their ionic conductivity is related to the concentration of O vacancies.[38] Since the ΔE_{VO} decreases with the increase of the mole fraction of Ca^{2+}, the doping of Ca^{2+} can, therefore, improve their ionic conductivities.

Conclusions

In summary, our first principles GGA+U results confirmed that the resistance of $NdFeO_3$ can be colossally reduced by the doping of Ca^{2+} cations. The structural and electronic analyses have been performed to give fundamental insight into the conductive properties of $Nd_{1-x}Ca_xFeO_{3-\delta}$ (x=0.00, 0.25, 0.50, 0.75 or 1.00, δ=0.00 or 0.25). For $Nd_{1-x}Ca_xFeO_3$ (x=0.00, 0.25, 0.50, 0.75 or 1.00), the hole states appear just above the Fermi level, implying a high mobility of electrons/holes along the Fe-O-Fe bonding network. Moreover, it has been found it becomes easier to form O vacancies with Ca substitution. The introduction of O vacancies make $Nd_{1-x}Ca_xFeO_{2.75}$ (x=0.00, 0.25, 1.00) compounds show a metallic behaviour. At the same time, we predict $Nd_{0.5}Ca_{0.5}FeO_{2.75}$ should have a large resistance with band gap of 1.47eV for balanced charge. Our calculations demonstrate that the introduction of lower-valence cations into $NdFeO_3$ can therefore provide an effective way to enhance both the electronic and ionic conductivity. These findings can help us to improve the conductance of such orthoferrities for practical applications, such as sensors, electrodes in SOFC.

Acknowledgements

This work was financially supported by the National Natural Science Foundation of China (Nos. 91022016, 21031005, 21231001, 11274222), National Key Basic Research Program of China (Grant No. 2015CB921600), program for Changjiang Scholars and Innovative Research Team in University (IRT 1207), QiMingXing and Pujiang Project (No. 14QA1402000) of Shanghai Municipal Science and Technology Commission, Eastern Scholar Program and Shuguang Program (No. 12SG34) from Shanghai Municipal Education Commission and the Fundamental Research Funds for the Central Universities, China (Grant No. FRF-SD-13-008A). This research was undertaken on the National Computational Infrastructure (NCI) in Canberra, Australia.

Notes and references

1. M. Idrees, M. Nadeem, M. Atif, M. Siddique, M. Mehmood and M. Hassan, *Acta Mater.*, 2011, **59**, 1338.
2. A. Jaiswal, R. Das, T. Maity and P. Poddar, *J. Appl. Phys.*, 2011, **110**, 124301.
3. W. Koehler, E. Wollan and M. Wilkinson, *Phys. Rev.*, 1960, **118**, 58.
4. L. Uba, S. Uba, L. Germash, L. Bekenov and V. Antonov, *Phys. Rev. B*, 2012, **85**, 125124.
5. J. Caicedo, J. Fontcuberta and G. Herranz, *Phys. Rev. B*, 2014, **89**, 045121.
6. Y. Tokunaga, N. Furukawa, H. Sakai, Y. Taguchi, T.-h. Arima and Y. Tokura, *Nat. Mater.*, 2009, **8**, 558.
7. Y. Tokunaga, S. Iguchi, T. Arima and Y. Tokura, *Phys. Rev. Lett.*, 2008, **101**, 097205.
8. Y. Tokunaga, Y. Taguchi, T. H. Arima and Y. Tokura, *Nat. Phys.*, 2012, **8**, 838.
9. J. Suntivich, K. J. May, H. A. Gasteiger, J. B. Goodenough and Y. Shao-Horn, *Science*, 2011, **334**, 1383.
10. J. J. Xu, D. Xu, Z. L. Wang, H. G. Wang, L. L. Zhang and X. B. Zhang, *Angew. Chem. Int. Ed.*, 2013, **52**, 3887.
11. I. Hamada, A. Uozumi, Y. Morikawa, A. Yanase and H. Katayama-Yoshida, *J. Am. Chem. Soc.*, 2011, **133**, 18506.
12. M. M. Natile, A. Ponzoni, I. Concina and A. Glisenti, *Chem. Mater.*, 2014, **26**, 1505.
13. Z. Dai, C. S. Lee, B. Y. Kim, C. H. Kwak, J. W. Yoon, H. M. Jeong and J. H. Lee, *Appl. Mater. Inter.*, 2014, **6**, 16217.
14. R. Voorhoeve, D. Johnson, J. Remeika and P. Gallagher, *Science*, 1977, **195**, 827.
15. M. Pena and J. Fierro, *Chem. Rev.*, 2001, **101**, 1981.

16. H. T. Giang, H. T. Duy, P. Q. Ngan, G. H. Thai and N. N. Toan, *Sens. Actuators, B*, 2011, **158**, 246.
17. J. W. Yin, Y. M. Yin, J. Lu, C. Zhang, N. Q. Minh and Z.-F. Ma, *J. Phys. Chem.C*, 2014, **118**, 13357.
18. J. Shi, Y. Zhou and S. Ramanathan, *Nat. Commun.*, 2014, **5**, 4860.
19. H. Kozuka, K. Yamagiwa, K. Ohbayashi and K. Koumoto, *J. Mater. Chem.*, 2012, **22**, 11003.
20. C. H. Yo, I. Y. Jung, K. H. Ryu, K. S. Ryu and J. H. Choy, *J. Solid State Chem.*, 1995, **114**, 265.
21. Y. H. Chen, Y. J. Wei, H. H. Zhong, J. F. Gao, X. Q. Liu and G. Y. Meng, *Ceram. Int.*, 2007, **33**, 1237.
22. L. Chen, T. Li, S. Cao, S. Yuan, F. Hong and J. Zhang, *J. Appl. Phys.*, 2012, **111**, 103905.
23. S. Yuan, W. Ren, F. Hong, Y. Wang, J. Zhang, L. Bellaiche, S. Cao and G. Cao, *Phys. Rev. B*, 2013, **87**, 184405.
24. P. E. Blöchl, *Phys. Rev. B*, 1994, 50, 17953.
25. J. P. Perdew, K. Burke and M. Ernzerhof, *Phys. Rev. Lett.*, 1996, **77**, 3865.
26. V. I. Anisimov, J. Zaanen, and O. K. Andersen, *Phys. Rev. B*, 1991, **44**, 943.
27. K. Momma, F. Izumi, *J. Appl. Crystallogr.* 2008, **41**, 653
28. M. Marezio, J. Remeika and P. Dernier, *Acta Crystallogr B,* 1970, **26**, 2008.
29. I. Ahmad, M. Akhtar, M. Younas, M. Siddique and M. Hasan, *J. Appl. Phys.*, 2012, **112**, 074105.
30. R. Pushpa, D. Daniel and D. P. Butt, *Solid State Ionics*, 2013, **249**, 184.
31. A. B. Muñoz-García, D. E. Bugaris, M. Pavone, J. P. Hodges, A. Huq, F. Chen, H. C. zur Loye and E. A. Carter, *J. Am. Chem. Soc.*, 2012, **134**, 6826.
32. W. Sławiński, R. Przeniosło, I. Sosnowska and E. Suard, *J. Phys.: Condens. Matter,* 2005, **17**, 4605.
33. R. F. W. Bader, *Atoms in Molecules - A quantum theory*, Oxford University Press, New York, 1990.
34. J. Suntivich, W. T. Hong, Y. L. Lee, J. M. Rondinelli, W. Yang, J. B. Goodenough, B. Dabrowski, J. W. Freeland and Y. Shao-Horn, *J. Phys. Chem.*C, 2014, **118**, 1856.
35. H. L. Tuller, *Solid State Ionics*, 1997, **94**, 63.
36. A. M. Ritzmann, A. B. Muñoz-García, M. Pavone, J. A. Keith and E. A. Carter, *Chem. Mat.*, 2013, **25**, 3011
37. M. Pavone, A. M. Ritzmann and E. A. Carter, *Energ. Environ. Sci.*, 2011, **4**, 4933.
38. A. B. J. A. Kilner, J. Rossiny, *In Perovskite Oxide for Solid Oxide Fuel Cells*, Springer, New York, 2009.